Permeability of DOPC Bilayers under Photoinduced Oxidation: Sensitivity to Photosensitizer

Isabel O. L. Bacellar,[a] Mauricio S. Baptista,[a] Helena C. Junqueira,[a] Mark Wainwright,[b] Fabrice Thalmann,[c] Carlos M. Marques,[c] André P. Schroder,[c*]

[a]: Departamento de Bioquímica, Instituto de Química, Universidade de São Paulo, 05508-000, São Paulo, Brazil.

[b]: School of Pharmacy & Biomolecular Sciences, Liverpool John Moores University, Liverpool L3 3AF, United Kingdom.

[c]: Institut Charles Sadron, Université de Strasbourg, CNRS UP22, 23 rue du Loess, 67200, Strasbourg, France.

*Corresponding author; email address: schroder@unistra.fr

Abstract

The modification of lipid bilayer permeability is one of the most striking yet poorly understood physical transformations that follow photoinduced lipid oxidation. We have recently proposed that the increase of permeability of photooxidized 1,2-dioleoyl-*sn*-glycero-3-phosphocholine (DOPC) bilayers is controlled by the time required by the oxidized lipid species to diffuse and aggregate into pores. Here we further probe this mechanism by studying photosensitization of DOPC membranes by methylene blue (MB) and DO15, a more hydrophobic phenothiazinium photosensitizer, under different irradiation powers. Our results not only reveal the interplay between the production rate and the diffusion of the oxidized lipids, but highlight also the importance of photosensitizer localization in the kinetics of oxidized membrane permeability.

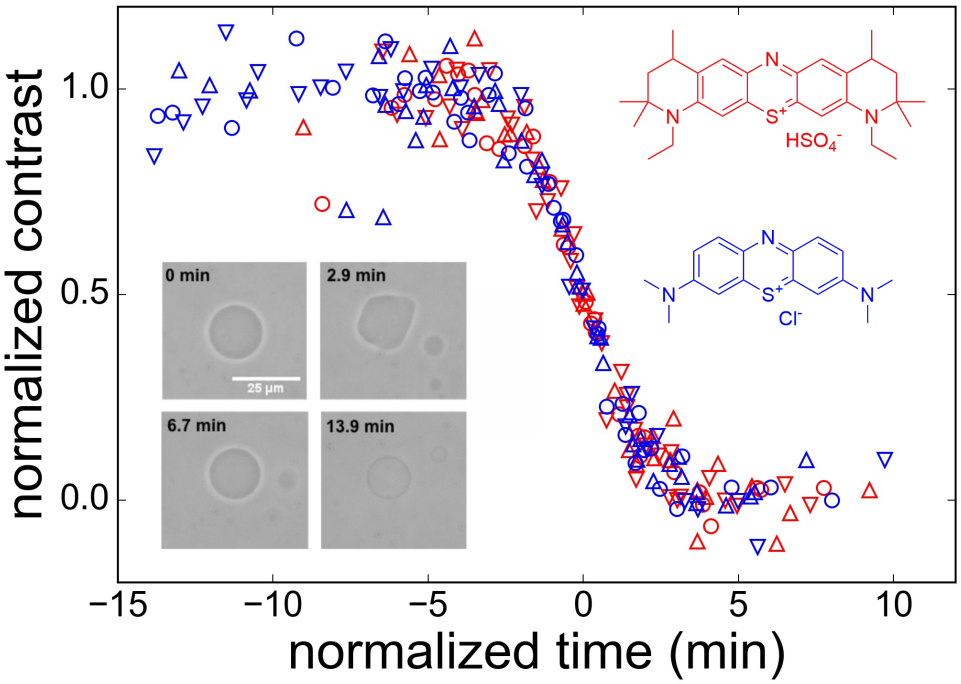

Keywords: model membrane, lipid photooxidation, pore formation, membrane permeabilization, phenothiazinium photosensitizers.

1. Introduction

Oxidation of lipid membranes is involved in a variety of phenomena relevant to several medical conditions, including neurodegenerative diseases[1] and cancer.[2] Lipid membrane oxidation can trigger cell signaling mechanisms[3] as well as inflict membrane permeabilization,[4, 5] which is one of its most striking cytotoxic consequences. Membrane permeabilization is a key step in the mechanisms of photodynamic therapy (PDT), a clinical modality that uses photosensitizers, light and oxygen to damage diseased cells by producing oxidized biomolecules.[6] In the case of lipids, oxidized species (e.g. lipid hydroperoxides) challenge cell homeostasis by markedly affecting the biophysical properties of membranes, including their capability to sustain chemical gradients.[6,7] To date PDT protocols remain however largely empirical and, by lacking support from detailed mechanistic data, fail to attain maximum efficiency with minimum side effects. Uncovering details of the kinetics of membrane permeabilization and understanding how this phenomenon is affected by light dose, photosensitizer concentration and chemical properties is therefore an essential step towards the development of PDT protocols resulting in specific biological effects.

Permeabilization of lipid bilayers under photooxidation occurs via pore opening, [4] a mechanism that is favored by oxidized lipids in a number of ways. Compared to bilayer forming lipids that have two similar or identical carbon tails and thus a packing parameter[8] consistent with planar self-assembling, lipids with a truncated tail favor instead micelle-like structures.[9, 10] Molecular dynamics simulations show that these features are encountered for instance in phospholipid aldehydes, oxidized products bearing a long carbon chain and a shorter aldehyde-bearing chain. Not only aldehydes bear packing parameters that stabilize pore rims, but also they are more polar and display higher chain mobility if compared with their non-oxidized precursors.[9,10] As the simulations show, if a few of these molecules are initially randomly positioned in a standard phospholipid bilayer, aggregates of phospholipid aldehydes form after a certain time and induce pore opening.[10] Experimentally, membranes self-assembled from mixtures of standard phospholipids and phospholipid aldehydes have also been shown to display increased permeability with respect to the uncharged fluorescent molecule PEG12-NBD[11,12] and to K^+.[13]

We have recently proposed that the increase in permeability of photooxidized 1,2-dioleoyl-*sn*-glycero-3-phosphocholine (DOPC) bilayers is controlled by the time required by the oxidized lipid species to diffuse and aggregate into pores,[4] an effect that was studied by microscopic observation of giant unilamellar vesicles (GUVs). This diffusion-limited mechanism provides for explicit predictions for the variation of permeabilization kinetics with photosensitizer concentration and also with light power. The predicted dependence on photosensitizer concentration was confirmed in our previous

work for the phenothiazinium dye methylene blue (MB),[4] a photosensitizer that has been successfully employed to treat conditions ranging from melanoma to severe bacterial and viral infections.[14-16] Herein, we first test the predicted dependence of permeabilization kinetics with irradiation power. Notably, tuning irradiation power allows modulating permeabilization kinetics under constant chemical composition, a clear advantage for many photosensitizers displaying concentration-dependent photochemistry due to aggregation effects.[17-19] Next, we evaluate if our predictions are also valid for a more hydrophobic phenothiazinum photosensitizer, DO15. By binding to membranes more extensively, DO15 was shown to induce membrane permeabilization faster than MB[19] and also to allow for high light/dark cytotoxicity ratios in biological context.[20-26] Our results highlight the importance of considering photosensitizer spatial distribution to PDT protocols, while shedding light on the permeabilization mechanism of photooxidized lipid bilayers.

2. Materials and Methods

2.1 Materials

5(6)-Carboxyfluorescein (CF), diethylenetriaminepentaacetic acid (DTPA), glucose, methylene blue (MB), Sephadex G-50, sodium dodecyl sulfate (SDS), sucrose, glucose and Triton X-100 were purchased from Sigma Aldrich. Chloroform, hydrochloric acid, sodium chloride, sodium hydroxide and tris(hydroxymethyl)aminomethane (Tris) were purchased from Labsynth. 1,2-Dioleoyl-*sn*-glycero-3-phosphocholine (DOPC) was purchased from Avanti Polar Lipids. DO15 was synthesized as in Wainwright *et al*.,[22] Milli-Q water (Millipore) was employed in all circumstances. The molecular structures of the photosensitizers are shown in Figure 1.

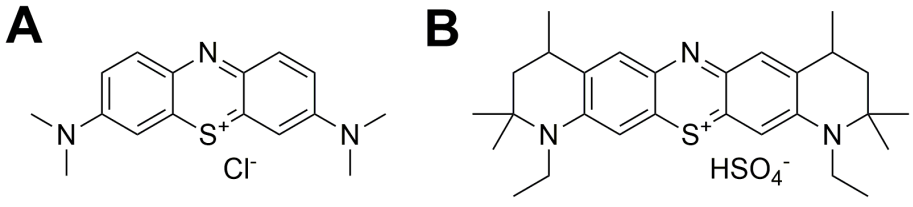

Figure 1: Molecular structures of (A) MB and (B) DO15.

2.2 Membrane binding

Similarly to a previous study in which soy lecithin liposomes were used,[19] PS binding to DOPC membranes was characterized from PS partitioning between membrane and aqueous solution by equilibration with liposomes and separation of bound and free PS by centrifugation.

DOPC vesicles were prepared as follows: 7.5 mg of DOPC were dissolved in chloroform, which was dried with an argon flow yielding a lipid film. A liposome suspension was obtained by hydration with 2 mL of 5 mM Tris buffer (pH = 7.6) and the mixture was agitated vigorously for 3 min. The suspension was then centrifuged for 10 min at 16000 g and the supernatant containing the smaller liposomes was discarded. The remaining pellet was re-suspended with 2 mL of the same buffer. This procedure was repeated three times to obtain a suspension of liposomes that sedimented well under centrifugation. Samples were prepared with 30 µL of the resulting suspension and enough buffer and photosensitizer in order to obtain 15 µM photosensitizer in 1 mL volume, corresponding to a PS/DOPC ratio of 10.5 mol%. After 1 h incubation, samples were centrifuged at 16000 g for 10 min, to separate the liposomal (containing bound PS) and aqueous fractions. The supernatant was collected and diluted with a 50 mM SDS solution containing 10% of Triton X-100 to avoid the presence of PS aggregates. The absorbance of the unbound dye (Abs_s) was compared to a sample lacking liposomes (Abs_0) in order to calculate the distribution ratio $P_{m/s}$ between the membrane and the aqueous solution, $P_{m/s} = (Abs_0 – Abs_s)/Abs_s$.

2.3 Liposome leakage assay

The leakage of material from the inner compartment of liposomes was assessed using the fluorescent probe 5(6)-carboxyfluorescein (CF). When CF is present only inside the liposomes at a sufficiently high concentration, self-quenching occurs and the sample is poorly emissive. However, leakage of CF to the outer solution results in dilution and consequent emission intensity enhancement.[27] The procedure was based on Bacellar *et al.*,[19] with a few modifications. 15 mg of DOPC were

dissolved in chloroform, which was dried with an argon flow yielding a lipid film. The film was hydrated with 0.5 mL of a 50 mM CF solution in 10 mM Tris buffer (pH=8.0). The suspension was extruded using a 50 nm pore-diameter membrane (Avanti Lipids, USA) and eluted in a Sephadex G-50 column equilibrated with 10 mM Tris buffer (pH=8.0) containing 0.3 M NaCl and 0.1 mM DTPA. The fraction containing liposomes was collected and used to prepare samples composed of 15 μL of liposome suspension and enough buffer and photosensitizer in order to obtain a 15 μM photosensitizer concentration and a total volume of 300 μL. Samples were placed in a 96-well microplate and irradiated with a LED array emitting at 631 nm (full width at half maximum of 18 nm) with 72 W m^{-2} irradiance. Fluorescence emission was detected with a SpectraMax i3 microplate reader (Molecular Devices, USA) with excitation and emission wavelengths set at 485 and 517 nm, respectively.

2.4 GUV leakage assay

Giant unilamellar vesicles (GUVs) were grown by the electroformation method.[28] 5 μL of a 1 g L^{-1} DOPC solution in chloroform were spread over the conducting face of each of two ITO-coated glass slides. Chloroform was evaporated under vacuum for 45 min. Sigillum Wax (Vitrex, Denmark) was placed around the lipid film on one of the slides and the second slide was used to assemble a chamber. The compartment was then filled with a 0.1 M sucrose solution and the glass slides were connected to an alternate current source (Agilent 33120) with 10 Hz frequency and 1 V tension for 2.5 h. Aliquots of the resulting GUV sample were diluted 10-fold with 0.1 M glucose solution containing enough photosensitizer to have a final photosensitizer concentration of 4 μM, and let in the dark at 4°C until being used for microscopy experiments. Osmolarities of glucose and sucrose were matched using a cryoscopic osmometer (Osmomat 030, Gonotec, Germany).

Coverslips separated by a spacer (Coverwell Perfusion Chambers PC4L-2.0, Grace Bio-Labs) were used for observation under an Eclipse TE 200 inverted microscope (Nikon) with a phase contrast (Ph-C), Plan Fluor ELWD 40x/0.60 objective

(Nikon). A digital camera (1800 NI-DIAG, Diagnostic Instruments Inc., USA) and a homemade software were used to acquire images. The sample was irradiated with the microscope mercury lamp (HBO 103W/2, see Figure SM-1 for spectrum), which maximum intensity (I~15 kW m^{-2}, no color filter) could be reduced 4- (I/4) or 8-fold (I/8) by neutral filters. We checked that, in absence of photosensitizer (MB or DO15), continuous illumination of the sample with the mercury lamp or with the halogen lamp used for observation (Ph-C mode) did not generate any GUV leakage in the experiment timescale. Each experiment started by selecting a region of the sample that contained at least one GUV (Figure 2, 0 min). The figure shows that the sugar-induced differences in refractive index result in an intensity contrast between the GUV interior and the surrounding solution, an essential feature for membrane permeability measurements, as explained below. Video acquisition was started under halogen lamp illumination (Ph-C mode), and kept active for the rest of the experiment. Consecutive sequences of irradiation (mercury lamp) and observation (Ph-C mode) of the sample were performed: the shutter of the HBO lamp was set opened, letting the light to reach the sample during a period over which the camera acquired saturated, white images; after some time, the shutter was closed so that images of the GUVs were acquired in the Ph-C mode during several seconds (Figure 2, 2.9 min and 6.7 min). The experiment was stopped when the GUV(s) had evolved through a stable state, characterized by no apparent difference of contrast with the surrounding solution (Figure 2, 13.9 min). Typically, experiments ran over minutes, up to twenty minutes, depending on the light intensity. The analyses of the recorded movies were carried out using a homemade software. The sequences of white, saturated images were used as the indication of the irradiation periods, with a typical time scale precision of 0.2 s. Phase contrast images taken during the non-irradiating periods were used to measure the average contrast between the GUVs and the outer solution, as already depicted elsewhere.[4] Briefly, intensity linear profiles (6 pixels width) were traced through the vesicle diameter, and the ‘Contrast’ was defined as the difference between maximum and minimum intensity of the profile (Figure 3A and B). Fig. 3C shows a typical evolution of ‘Contrast’ as a function of time. Irradiation periods correspond to time

sequences with no Contrast. Noteworthy, 'Contrast' shows no evolution during the periods in Ph-C mode, which lasted 5-10 s (see Fig. 3D). In comparison, irradiation periods were of 1-3 min, meaning that cumulated irradiation times were circa 100-fold that of the cumulated non-irradiation times. This observation discards the possibility that membrane oxidation significantly progresses during observation periods and specifically that dark reactions derived from Type I chemistry further progressed whilst Type II reactions would be halted by lack of irradiation. As such, 'Contrast' can be plotted as a function of the cumulative irradiation time, as discussed later, and Boltzmann sigmoidal functions were fitted (Origin Lab 8.0) to the resulting curves.

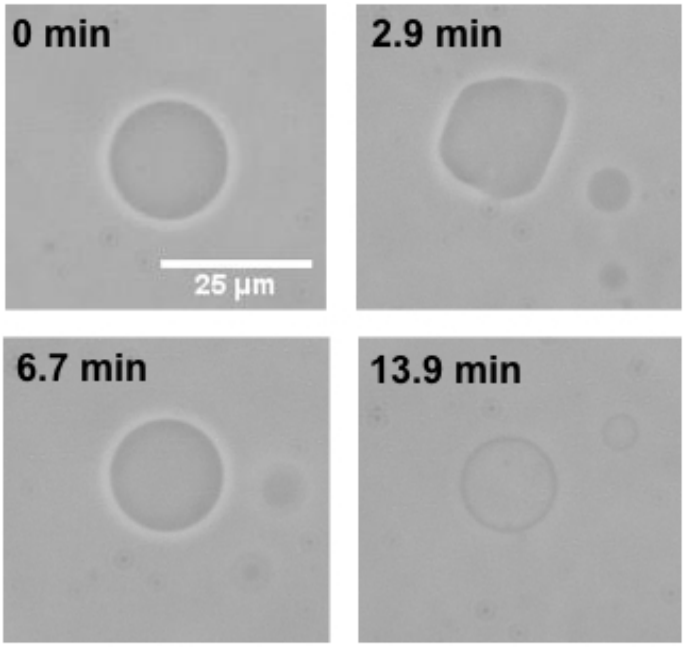

Figure 2: Phase contrast microscopy images of a DOPC GUV in a 4 µM MB solution, irradiated with the light intensity I/8, at different irradiation times (t=0, 2.9, 6.7, and 13.9 min).

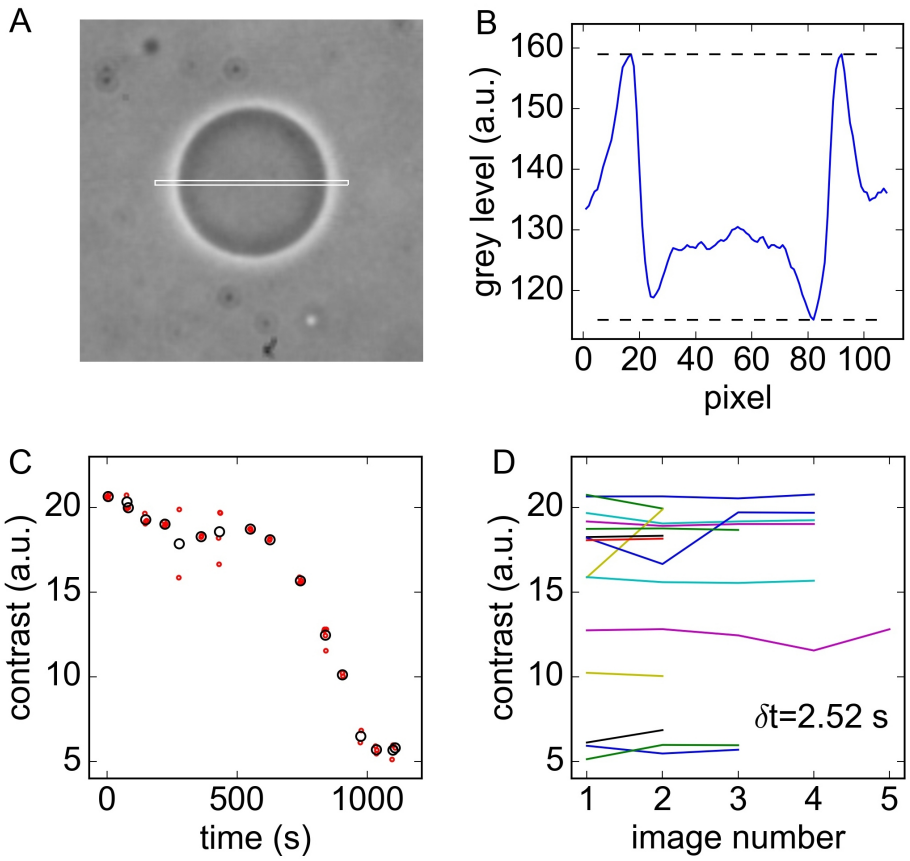

Figure 3: A: Typical phase contrast image of a GUV, here with an adjusted contrast, and scheme of the 6 pixel height diametral rectangle. Image width is 70 µm. B: averaged intensity profile along the rectangle defined in A. The difference between maximum and minimum profile (dotted lines) is defined as the 'Contrast'. C: 'Contrast' as a function of time for a GUV in 4 µM of MB, for irradiation at I/4. Small circles correspond to individual images, like in B, big circles are averages over 'non-irradiation' sequences. D: Individual 'Contrast' values measured in C, as a function of image position in a 'non-irradiation' sequence. Acquisition frame rate is 0.4 frame/s. Values are connected by lines for visualization help.

3. Results

$P_{m/s}$, the distribution ratio of photosensitizer between the membranes and the solution was determined for MB and DO15 in DOPC liposomes, yielding values of 0.03±0.04 and 1.8±0.1, respectively. Unlike MB, that barely binds to liposomes, partitioning of DO15 favors its binding to the DOPC membrane. Such higher affinity of DO15 for the DOPC membrane is in qualitative agreement with results obtained by Bacellar *et al.* for membranes reconstituted from soy lecithin (SL),[19] i.e. 0.06±0.01 and 13±9 for MB and DO15 respectively. The 6-fold difference observed with DO15 for SL

when compared to DOPC can be attributed to the SL composition. Indeed, SL contains various phospholipid classes, being a mixture of phosphatidylcholine (PC), phosphatidylinositol (PI), phosphatidic acid (PA), and phosphatidylethanolamine (PE), besides containing fatty acids with various chain lengths, and unsaturation levels.[29, 30]

That DO15 interacts with membranes more extensively than MB was confirmed by measuring the leakage of a fluorescent probe entrapped in DOPC liposomes, which shows emission enhancement upon dilution in the outer solution. As shown in Fig SM-2, while no leakage was observed for MB over the experiment time scale, DO15 induced a clear leakage process. These results are in agreement with those obtained in the previous soy-lecithin based study, in which MB did not lead to a significant leakage in SL liposomes, while DO15 induced 100% leakage after the same irradiation period.[19]

While only DO15 was able to permeabilize liposomes, both MB and DO15 were able to promote GUV membrane permeabilization even in short time ranges of a few tens of minutes. This effect can be accounted both to the greater light power used for GUV irradiation (SM) and to GUV geometry, which leads to a situation with a much larger photosensitizer to lipid concentration ratio in comparison to LUV experiments. We checked that Hg irradiation did not induce any membrane modification of DOPC GUVs in absence of PS. As exemplified in Figure 2 for MB, irradiation of DOPC GUVs immersed in a 4 μM MB or DO15 solution led in both cases to vesicle morphological changes similar to those reported for MB and other photosensitizers.[4,31-34] Phase contrast microscopy demonstrates how initially round-shaped GUVs evolve towards more irregular, fluctuating shapes after some irradiation time. However, as irradiation continues, GUVs eventually recover a spherical shape, starting to lose their contrast with respect to the outer solution (Figure 2, 13.9 min). During this second step, pores with sizes above several micrometers have been sometimes observed (Figure 4), as already reported elsewhere.[4,35] As claimed elsewhere, membrane pore opening in such aqueous environment are not typically resolvable, except under particular conditions including a decrease in pore line tension, as expected from the accumulation of oxidized lipids.[35] Several molecular simulation studies have reported

that oxidized lipids, in particular phospholipid aldehydes, are able to promote pore opening in bilayers.[9,10,36] We hypothesize that pores are at the origin of the observed loss of contrast, being mostly of sub-optical sizes, *i.e.* non-detectable by optical microscopy.

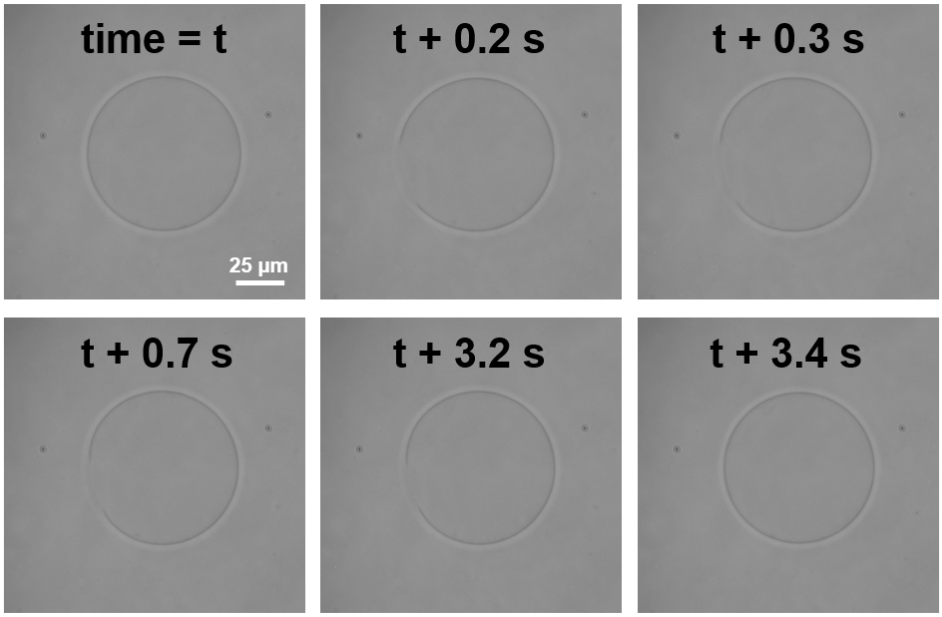

Figure 4: Membrane pore captured for a GUV under irradiation (light intensity = I) with 4 µM DO15, showing a pore from t+0.2 s of irradiation, after the end of the strong shape fluctuations period.

"Contrast" values as a function of the cumulative irradiation time were plotted for GUVs irradiated with MB or DO15 under different light intensities (I, I/4 and I/8) (Fig. 5A-F). All the profiles of contrast versus time can be well fitted by the Boltzmann function:

$$\text{Contrast} = A_2 + (A_1 - A_2)/[1 + e^{((t-\tau)/\Delta\tau)}] \qquad (1)$$

where A_1 and A_2 correspond to the initial and final contrast values respectively, τ is the half decay time, and $d\tau$ is the width of the distribution. Fig. 5A-F clearly show that there is a difference between MB and DO15 in the range of timescales required for GUVs to lose contrast, DO15 inducing faster kinetics than MB, as will be further discussed below. Figure 5G shows the same plots where the Contrast is normalized by its initial

and final values A_1 and A_2 (*i.e.* plotted as (Contrast-A_2)/(A_1-A_2)), and the time evolution is centered at zero and normalized by the time width $\Delta\tau$ (*i.e.* plotted as a function of (t-τ)/$\Delta\tau$).

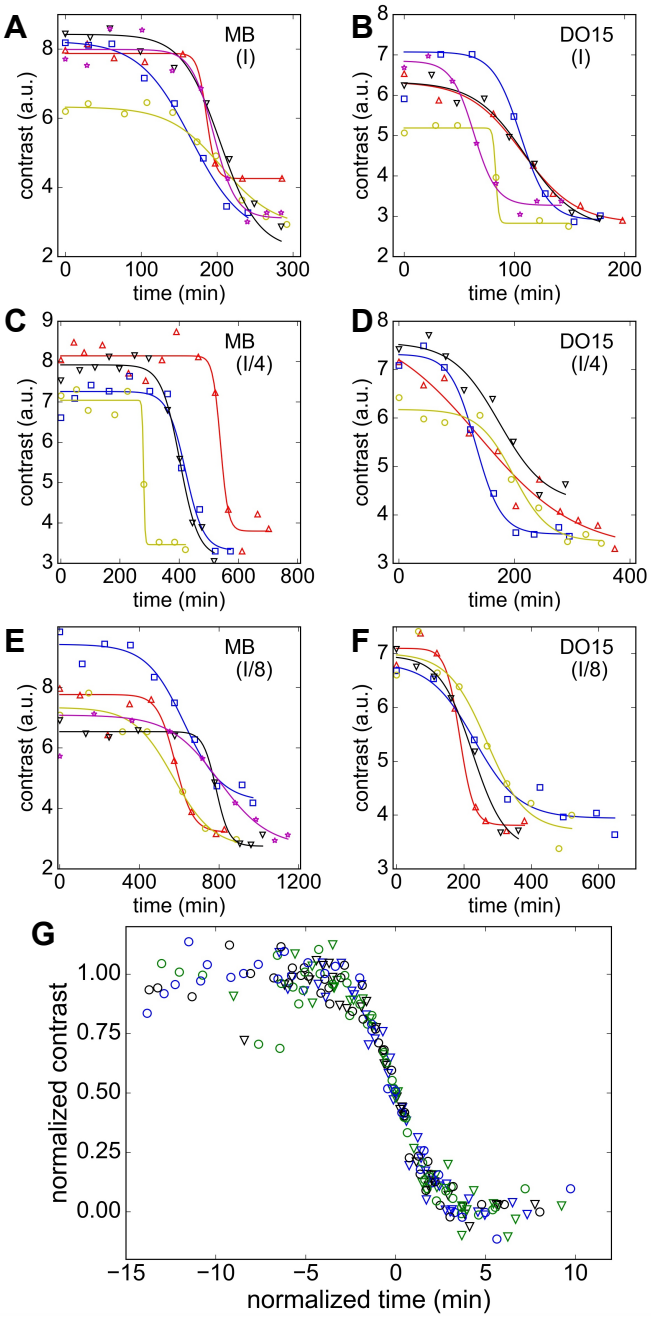

Figure 5: (A-F) Variation of the 'Contrast' as a function of irradiation time for GUVs irradiated with 4 µM MB or DO15 under different light intensities. Each color shade corresponds to an experiment with a different GUV. That all normalized time profiles follow well a Boltzmann function is shown in (G), where all data collapse in a single master plot. Circles are for MB, triangles for DO15, black, blue, and green are for I, I/4, and I/8 respectively.

4. Discussion

DOPC membrane permeabilization by MB or DO15 was studied by optical contrast induced by sugar asymmetry in GUVs. DO15 was more efficient than MB, in agreement with irradiation-induced leakage of liposomes made of both soy lecithin membranes[19] or DOPC (S.M. section). Experiments on GUVs enable monitoring the behavior of a single membrane during the lipid oxidation process, taking advantage of higher irradiation power and larger photosensitizer to lipid concentration ratio. MB and DO15 were used at a 4 μM concentration, at which aggregation, a common trend for such molecules, is know to be minimum, as demonstrated elsewhere.[17] Note that 4 μM was chosen since it enabled to observe and characterize GUV loss of contrast while still keeping overall irradiation times into a reasonable range of a few tens of minutes with both MB and DO15 (Fig. 5).

The morphological changes of the DOPC membrane displayed in Figure 2 are induced by irradiation in the presence of the photosensitizers. They were first reported by Caetano *et al.*[5] and since then identified as corresponding to different oxidation steps of the membrane. Among the possible lipid oxidation processes is the formation of lipid hydroperoxides by singlet oxygen: after singlet oxygen is formed by energy transfer from the triplet excited state of the photosensitizer to ground state molecular oxygen, singlet oxygen can directly react with unsaturated lipids via the ene reaction and yield lipid hydroperoxides.[37] Formation of DOPC hydroperoxides leads to an increase in the area per lipid of about 20%,[31] explaining the strong fluctuations first observed. However, hydroperoxidation does not lead to membrane disruption or permeability increase with respect to sucrose or glucose, as proven by the preservation of GUV optical contrast[31] and endorsed by molecular dynamics simulations.[10,38,39] Further oxidation beyond hydroperoxidation eventually results in different lipid species, including phospholipids with one or two carbon short chains and bearing aldehyde and other groups. These oxidized lipids with one or two short carbon chains were shown to increase membrane permeability in molecular dynamics simulations through pore-opening[9,10,36] and have also been shown to increase the permeability of membranes

already assembled from these molecules.[11-13] The formation of truncated phospholipids was hypothesized by Caetano *et al.*, who observed that irradiation of lipid suspensions with high concentrations of MB (> 50 μM) also led to liposome destruction and decrease in surface tension of the air-water interface.[5] The latter effect was attributed to formation of short chain carboxylic acids, as a result of phospholipid fatty acyl chain cleavage.[5] We will refer to such oxidized lipids, capable of membrane permeabilization as “pore-forming lipids”. Since they are randomly generated in the membrane, the formation of a pore first requires diffusion and aggregation. We have previously computed the consequences of this scenario for the kinetics of pore formation.[4] As illustrated in Figure 6, central to our prediction is the time required to form an aggregate with n pore-forming lipids, given by the following equation[4]

$$n = 2\pi D\alpha\ t^2 \frac{1}{\ln\left(t/t_0\right)} \qquad (2)$$

where D is the lipid’s diffusion coefficient, α the rate of oxidation of pore-forming lipids per unit area of membrane and t_0 the time required for a lipid to explore a pore size R_P. The factor αt^2 is a direct consequence of assuming a constant production rate for the oxidized lipids, and in the simple case where a photosensitizer does not interact with the membrane, the production rate α is expected to be proportional to bulk photosensitizer concentration C_{PS} and light intensity I, *i.e.* $\alpha \sim C_{PS}$ I. Note that the proportionality of α with C_{PS} holds even though only singlet oxygen $^1O_2$ generated in a layer of 100 nm width on both sides reaches the membrane.[5] Indeed, that thickness corresponds to the diffusion length $\delta=(D\tau)^{1/2}$ of $^1O_2$, with $D=3\times10^{-5}$ cm^2 s^{-1} the diffusion coefficient of $^1O_2$,[40] and $\tau=3\times10^{-6}$ s its decay time in water.[41] Given a value n_0 of oxidized lipids required to form a pore, inversion of Equation 2 provides an equation for the permeation time, *i.e.* the experimentally-determined parameter τ, as a function of C_{PS} and I. In the present study, C_{PS} is constant, and I is the experimental variable; one gets from Equation 2:

$$I \propto \frac{n_0}{2\pi D\ C_{PS}} \frac{1}{\tau^2} \ln\left(\frac{\tau}{\tau_0}\right) \qquad (3)$$

We have previously shown for a MB/DOPC system that the dependence of permeation time with MB concentration C_{MB} follows approximately the expected scaling law $\tau \sim C_{MB}^{-1/2}$. Figure 7A presents the evolution of τ with the light power, for MB and DO15. In the case of MB, τ follows the expected variation law $\tau \sim I^{-1/2}$ (dash-dotted line) closely, in agreement with our previous analyses described above[4] i.e. with eq.(3). Figure 7A further demonstrates that a better fit is obtained by using the full expression in Equation 3 (Figure 7A and B, thin blue dashed line), which includes also the logarithmic term that is neglected in the scaling approximation. The best fit using Equation 3 gives the value t_0 = 2.2 s, from which an average pore size $R_P \approx 1$ µm can be extracted ($R_P = (Dt_0)^{0.5}$), assuming a typical diffusion coefficient for the oxidized lipid species D = 1 µm^2 s^{-1}.[42,43] In practice, only a few pores larger than 1 µm were observed in some of our experiments, as the one shown in Figure 4. Runas and Malmstadt reported that pores in the nanometer size range were formed in GUVs containing up to 12.5% (mol%) of the oxidized lipid 1-palmitoyl-2-(9'-oxo-nonanoyl)-*sn*-glycero-3-phosphocholine; indeed GUVs were permeable to PEG12-NBD, but not to 40 or 2000 kDa fluorescein-dextran. However, the authors also reported that pores with diameters larger than 55 nm can be formed for larger amounts of oxidized lipid, leading to permeability to fluorescein-dextran.[11] This indicates that pores of larger sizes can form as an increasing number of oxidized lipids is generated.

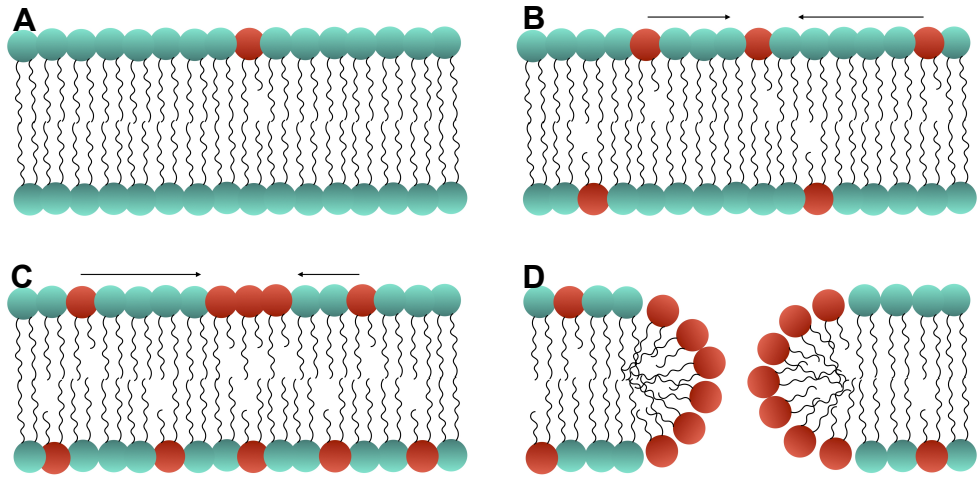

Figure 6: (A) seed pore-forming lipid being formed in the membrane, from the reference of which other lipids diffuse towards it. (B), (C) pore-forming lipids diffusion and aggregation on the reference lipid. (D) active pore, formed once the pore seed has n_0 lipids.

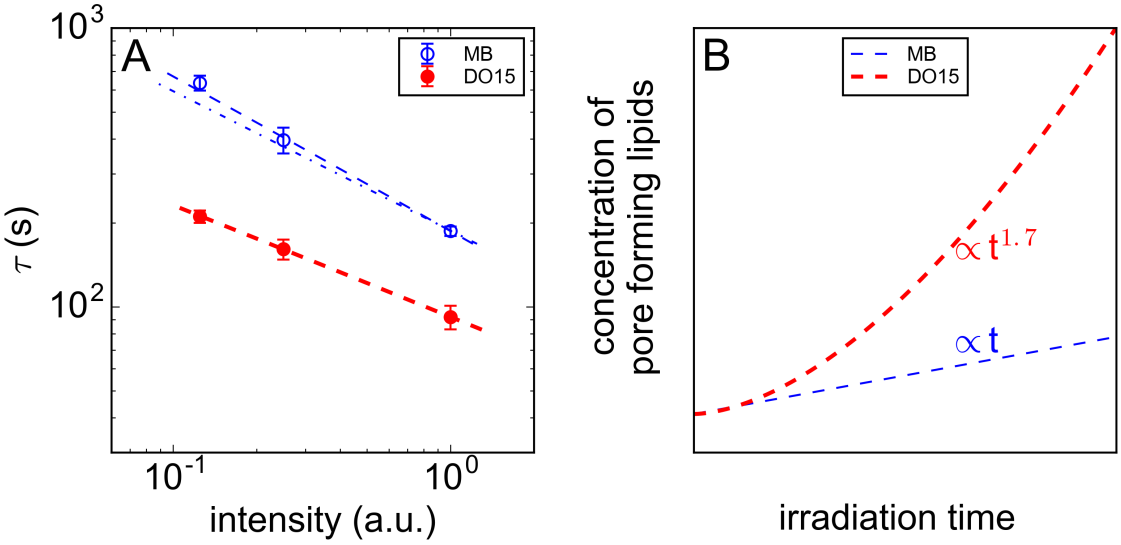

Figure 7: (A) circles correspond to characteristic time τ for contrast loss extracted from fitting the data in Figure 5A-F with the Boltzmann equation (Equation 1). Lines correspond to fits: dash-dotted (MB) is for a simple $n \sim t^2$ law; thin, dashed (MB) is for Equation 3, giving $t_0 = 2.2$ s; thick, dashed (DO15) is for a modified Equation 3 with imposed $t_0 = 2.2$ s, and variable power law for (t), obtained for the power law $n \sim t^{2.7}$, i.e. $I \sim t^{-2.7}$. (B) Schematic representation of the formation of pore-forming lipids; while constant for MB, the rate of production of these lipids in presence of DO15 grows as $t^{0.7}$. As shown in the figure, this corresponds to a concentration of oxidized lipids growing as t in presence of MB or $t^{1.7}$ for DO15.

Contrary to MB, the permeation time $\tau(I)$ measured with DO15 cannot be fitted by Equation 2. An acceptable fit (displayed in Figure 7A) can nevertheless be obtained by changing the power of the time dependence of Equation 2 from $n \sim t^2$ to $n \sim t^{2.7}$ ($I \sim \tau^{-2.7}$ in Equation 3). Assuming still a diffusion-limited pore formation, such dependence would point to a rate of generation of the pore-forming species that is not constant, but grows rather as $t^{0.7}$. These results are summarized in Figure 7B. While a constant rate of production of the pore-forming lipids such as that observed for MB is a natural mechanism to consider, the time-increasing rate that would explain permeabilization under DO15 is somewhat more complex. An obvious difference between the two sensitization environments is the larger observed affinity of DO15 for the lipid membranes. Assuming that pore-forming lipids are generated by reactions involving the triplet states of the photosensitizer, one would have thus for MB a creation of triplets by illumination of molecules in the solution in the neighborhood of the membrane, with reactions between the triplets and the lipids occurring only for those rare MB molecules coming into close distance of a lipid unsaturated bond. Since the reactions are scarce the generation of pore-forming lipids is limited by the rate of reaction, with a constant rate of production. Contrary to MB, there is a significant amount of DO15 in the membrane ($P_{m/s}$=1.8 in DOPC liposomes), and the reactions are likely to involve predominantly triplet states generated in those DO15 molecules already in the bilayer. An obvious implication is that the renewal of the DO15 molecules consumed by the reactions will in this case play a role in the kinetics of generation of pore-forming lipids. Although studies on DO15 adsorption kinetics are beyond the scope of this paper, it is tempting to speculate at this point that such kinetics processes play an important role in the permeabilization generated by DO15 photosensitization.

5. Conclusions

In previous studies of lipid oxidation by the photosensitizer MB,[4] we proposed a reaction-diffusion mechanism to describe membrane permeabilization, encompassing the production of pore-forming lipids at a constant rate and their diffusion-limited aggregation leading to pores. The mechanism explains well the observed photosensitizer concentration-dependence of the time needed for GUV loss of contrast, and additionally predicts the dependence with light power. In the present paper we confirm the validity of the proposed mechanism, by showing that the variation of light power leads to the expected kinetics responses for MB. However, we also show that the kinetics of permeabilization are sensitive to the spatial distribution of the photosensitizer. DO15, a photosensitizer with a high affinity to the membrane displays a faster kinetics that MB, incompatible with a constant rate of formation of pore-forming lipids. Although the exact reaction pathways that lead to the generation in the membrane of pore-forming lipids is not yet known, it is very likely that such reactions involve the triplet states of the photosensitizers: indeed, pure hydroperoxidation does not compromise the permeability of the membrane.[11] We thus propose that differences in permeabilization kinetics between MB and DO15 are explained by the different spatial distributions of both photosensitizers and in particular by the time evolution of photosensitizer triple states available for the reactions.

Acknowledgments

Fundação de Amparo à Pesquisa do Estado de São Paulo (FAPESP) (2012/50680, 2013/07937-8, 2013/11640-0) and NAP-Phototech are acknowledged for financial support.

References

[1] Axelsen PH, Komatsu H, Murray IV. Oxidative stress and cell membranes in the pathogenesis of Alzheimer's disease. Physiology (Bethesda). 2011 Feb;26(1):54-69. doi: 10.1152/physiol.00024.2010.

[2] Giuseppina Barrera Oxidative Stress and Lipid Peroxidation Products in Cancer Progression and Therapy ISRN Oncol. 2012; 2012: 137289. Published online 2012 Oct 17. doi: 10.5402/2012/137289

[3] J.W. Zmijewski, A. Landar, N. Watanabe,D.A. Dickinson,N. Noguchi,and V.M. Darley-Usmar, Cell signalling by oxidized lipids and the role of reactive oxygen species in the endothelium, Biochem Soc Trans. 2005 Dec; 33(Pt 6): 1385–1389. doi: 10.1042/BST20051385.

[4] O. Mertins, I.O.L. Bacellar, F. Thalmann, C.M. Marques, M.S. Baptista, and R. Itri. Physical damage on giant vesicles membrane as a result of methylene blue photoirradiation. Biophys. J. (2014), 106: 162–171.

[5] W. Caetano, P.S. Haddad, R. Itri, D. Severino, V.C. Vieira, M.S. Baptista, A.P. Schröder, and C.M. Marques. Photo-induced destruction of giant vesicles in methylene blue solutions. Langmuir (2007), 23: 1307–1314.

[6] IOL Bacellar, TM Tsubone, C Pavani, MS Baptista Photodynamic efficiency: from molecular photochemistry to cell death International journal of molecular sciences 2015, 16 (9), 20523-20559

[7] Itri, R., Junqueira, H. C., Mertins, O., & Baptista, M. S. (2014). Membrane changes under oxidative stress: the impact of oxidized lipids. Biophysical reviews, 6(1), 47-61.

[8] Jacob N. Israelachvili, Intermolecular and Surface Forces, Academic Press, 2011.

[9] M. Lis, A. Wizert, M. Przybylo, M. Langner, J. Swiatek, P. Jungwirth, and L. Cwiklik. The effect of lipid oxidation on the water permeability of phospholipids bilayers. Physical Chemistry Chemical Physics (2011), 13(39): 17555.

[10] P. Boonnoy, V. Jarerattanachat, M. Karttunen, and J. Wong-ekkabut. Bilayer Deformation, Pores, and Micellation Induced by Oxidized Lipids. The Journal of Physical Chemistry Letters (2015), 6(24): 4884–4888.

[11] K.A. Runas, and N. Malmstadt. Low levels of lipid oxidation radically increase the passive permeability of lipid bilayers. Soft Matter (2015), 11(3): 499–505.

[12] K.A. Runas, S.J. Acharya, J.J. Schmidt, and N. Malmstadt. Addition of Cleaved Tail Fragments during Lipid Oxidation Stabilizes Membrane Permeability Behavior. Langmuir (2016), 32(3): 779–786.

[13] S. Ytzhak, and B. Ehrenberg. The effect of photodynamic action on leakage of ions through liposomal membranes that contain oxidatively modified lipids. Photochemistry and Photobiology (2014), 90(4): 796–800.

[14] Tardivo, J.P. et al. (2004). Treatment of melanoma lesions using methylene blue and RL50 light source. Photodiagnosis and Photodynamic Therapy, 1, pp.345–346.

[15] Tardivo, J.P., Wainwright, M. and Baptista, M.S. (2012). Local clinical phototreatment of herpes infection in São Paulo. Photodiagnosis and Photodynamic Therapy, 9(2), pp.118–121.

[16] Tardivo, J. P., Adami, F., Correa, J. A., Pinhal, M. A. S., & Baptista, M. S. (2014). A clinical trial testing the efficacy of PDT in preventing amputation in diabetic patients. Photodiagnosis and photodynamic therapy, 11(3), 342-350.

[17] H.C. Junqueira, D. Severino, L.G. Dias, M.S. Gugliotti, and M.S. Baptista. Modulation of methylene blue photochemical properties based on adsorption at aqueous micelle interfaces. Physical Chemistry Chemical Physics (2002), 4(11): 2320–2328.

[18] D. Severino, H.C. Junqueira, M. Gugliotti, D.S. Gabrielli, and M.S. Baptista. Influence of negatively charged interfaces on the ground and excited state properties of methylene blue. Photochemistry and Photobiology (2003), 77(5): 459–468.

[19] I.O.L. Bacellar, C. Pavani, E.M. Sales, R. Itri, M. Wainwright, and M.S. Baptista. Membrane damage efficiency of phenothiazinium photosensitizers. Photochem. Photobiol. (2014), 90: 801–813.

[20] Rodrigues, G. B., M. Dias‐Baruffi, N. Holman, M. Wainwright and G. U. L. Braga (2013) In vitro photodynamic inactivation of Candida species and mouse fibroblasts with phenothiazinium photosensitisers and red light. Photodiagn. Photodyn. Ther. 10, 141–149.

[21] Rodrigues, G. B., L. K. S. Ferreira, M. Wainwright and G. U. L. Braga (2012) Susceptibilities of the dermatophytes Trichophyton mentagrophytes and T. rubrum microconidia to photodynamic antimicrobial chemotherapy with novel phenothiazinium photosensitizers and red light. J. Photochem. Photobiol. B, Biol. 116, 89–94.

[22] Wainwright, M., K. Meegan and C. Loughran (2011) Phenothiazinium photosensitisers IX. Tetra‐ and pentacyclic derivatives as photoantimicrobial agents. Dyes Pigm. 91, 1–5.

[23] Wainwright, M., H. Smalley, O. Scully and E. Lotfipour (2012) Comparative photodynamic evaluation of new phenothiazinium derivatives against Propionibacterium acnes. Photochem. Photobiol. 88, 523–526.

[24] Ball, D. J., Y. Luo, D. Kessel, J. Griffiths, S. B. Brown and D. I. Vernon (1998) The induction of apoptosis by a positively charged methylene blue derivative. J. Photochem. Photobiol. B, Biol. 42, 159–163.

[25] Noodt, B. B., G. H. Rodal, M. Wainwright, Q. Peng, R. Horobin, J. M. Nesland and K. Berg (1998) Apoptosis induction by different pathways with methylene blue derivative and light from mitochondrial sites in V79 cells. Int. J. Cancer 75, 941–948.

[26] Peng, Q. A., S. B. Brown, J. Moan, J. M. Nesland, M. Wainwright, J. Griffths, B. Dixon, J. Crusesawyer and D. Vernon (1993) Biodistribution of a methylene‐blue derivative in tumor and normal‐tissues of rats. J. Photochem. Photobiol. B, Biol. 20, 63–71.

[27] J. Weinstein, S. Yoshikami, P. Henkart, R. Blumenthal, and W. Hagins. Liposome-cell interaction: transfer and intracellular release of a trapped fluorescent marker. Science (1977), 195 (4277): 489–492.

[28] M.I. Angelova, and D.S. Dimitrov. Liposome electroformation. Faraday Discuss. Chem. Soc. (1986), 81: 303.

[29] G. Wang G, and T. Wang. Oxidative Stability of Egg and Soy Lecithin as Affected by Transition Metal Ions and pH in Emulsion. J. Agric. Food Chem. (2008), 56: 11424–11431.

[30] R.H. Thornton, C.S. Johnson, and M.A. Ewan. The Component Fatty Acids of Soybean Lecithin. Oil & Soap (1944), 21(3): 85-87.

[31] G. Weber, T. Charitat, M.S. Baptista, A.F. Uchoa, C. Pavani, H.C. Junqueira, Y. Guo, V.A. Baulin, R. Itri, C.M. Marques, and A.P. Schroder. Lipid oxidation induces structural changes in biomimetic membranes. Soft Matter (2014), 10: 4241–4247.

[32] K.A. Riske, T.P. Sudbrack, N.L. Archilha, A.F. Uchoa, A.P. Schroder, C.M. Marques, M.S. Baptista, and R. Itri. Giant vesicles under oxidative stress induced by a membrane-anchored photosensitizer. Biophys. J. (2009), 97: 1362–1370.

[33] J. Heuvingh, and S. Bonneau. Asymmetric Oxidation of Giant Vesicles Triggers Curvature-Associated Shape Transition and Permeabilization. Biophys. J. (2009), 97: 2904–2912.

[34] R. Kerdous, J. Heuvingh, and S. Bonneau. Photo-dynamic induction of oxidative stress within cholesterol-containing membranes: Shape transitions and permeabilization. Biochim. Biophys. Acta. (2011), 1801: 2965–2972.

[35] S. Sankhagowit, S-H. Wu, R. Biswas, C.T. Riche, M.L. Povinelli, and N. Malmstadt. The Dynamics of Giant Unilamellar Vesicle Oxidation Probed by Morphological Transitions. Biochimica et Biophysica Acta (2014), 1838: 2615-2624.

[36] L. Cwiklik, and P. Jungwirth. Massive oxidation of phospholipid membranes leads to pore creation and bilayer disintegration. Chemical Physics Letters (2010), 486(4–6): 99–103.

[37] A.W. Girotti. Photosensitized oxidation of membrane lipids: Reaction pathways, cytotoxic effects, and cytoprotective mechanisms. Journal of Photochemistry and Photobiology B: Biology (2001), 63(1–3): 103–113.

[38] M. Yusupov, J. Van der Paal, E.C. Neyts, and A. Bogaerts. Synergistic effect of electric field and lipid oxidation on the permeability of cell membranes. Biochimica et Biophysica Acta - General Subjects (2017), 1861(4): 839–847.

[39] J. Van der Paal, E.C. Neyts, C.C.W. Verlackt, and A. Bogaerts. Effect of lipid peroxidation on membrane permeability of cancer and normal cells subjected to oxidative stress. Chem. Sci. (2016), 7(1): 489–498.

[40] B. A. Lindig, M. A. J. Rodgers. Rate Parameters for the Quenching of Singlet Oxygen by Water-Soluble and Lipid-Soluble Substrates in Aqueous and Micellar Systems. Photochem. Photobiol. (1981), 33(5): 627- 634.

[41] M.A.J. Rodgers, P.T. Snowden. Lifetime of o-2(1delta-g) in Liquid Water as Determined by Time-Resolved Infrared Luminescence Measurements. J. Am. Chem. Soc. (1982), 104(20): 5541- 5543.

[42] W.W. Webb. Applications of fluorescence correlation spectroscopy. Quarterly Reviews of Biophysics (1976), 9:49–68.

[43] A. Benda, M. Benes, V. Marecek, A. Lhotsky, W.T. Hermens, and M. Hof. How to determine diffusion coefficients in planar phospholipid systems by confocal fluorescence correlation spectroscopy. Langmuir (2003), 20:4120–4126.

Supplementary Material

Spectrum of the light source for GUV experiments

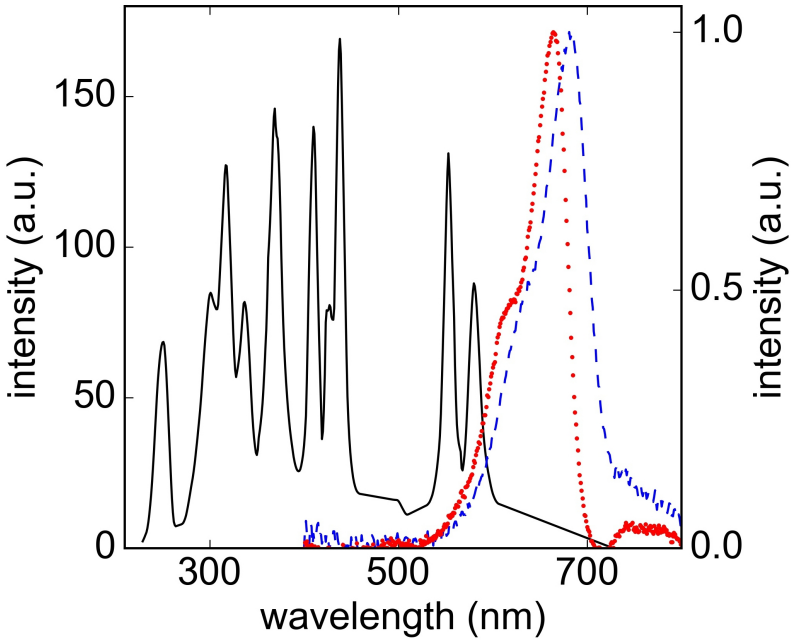

Figure SM-1: HBO lamp emission spectrum (continuous line), MB (dotted line) and DO15 (dots) absorption spectra. HBO total power corresponds to 15000 W m^{-2}.

Raw data for permeabilization kinetics in GUVs

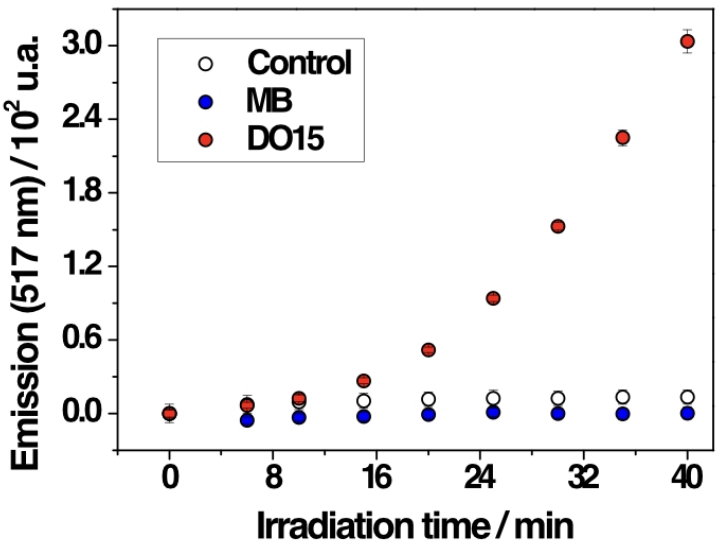

Figure SM-2: 5(6)-Carboxyfluorescein emission intensity at 517 nm as a function of irradiation time (631 nm LED, with 72 W m^{-2} irradiance), using DOPC liposomes and 15 μM photosensitizer in 10 mM Tris buffer (pH = 8) with 0.1 mM DTPA and 0.3 M NaCl.